Theoretical models to calculate stopping and ionization ratios of H_2^+ molecules in solid targets

C. D. Archubi*
Consejo Nacional de Investigaciones Científicas y Técnicas – Universidad de Buenos Aires, Instituto de Astronomía y Física del Espacio, Pabellón IAFE, 1428 Buenos Aires, Argentina
and Universidad de Buenos Aires, Facultad de Ciencias Exactas y Naturales, Departamento de Física, Ciudad Universitaria, 1428 Buenos Aires, Argentina

N. R. Arista†
Centro Atómico Bariloche and Instituto Balseiro, Comisión Nacional de Energía Atómica, 8400 S. C. de Bariloche, Argentina

(Received 21 December 2018; revised manuscript received 11 February 2019; published 7 March 2019)

In this work we study the vicinage effects that arise in the interaction of molecular projectiles with solids, considering, in particular, the effects produced by the excitation of inner shells. For this purpose, we use two different approaches. On one side we extend the use of the semiclassical impact-parameter model for the excitation of atomic shells, considering quantum corrections and the role of target screening in the vicinage effects. On the other hand, we adapt our extended wave-packet model, developed in a previous work to the calculation of stopping ratios and ionization cross sections for correlated ions. This model introduces modifications to the wave-packet method originally proposed by Kaneko, using the Levine and Louie technique to take into account the energy gaps corresponding to the different atomic levels of the target. Finally, we add the contribution of valence electrons calculated with the Lindhard free-electron-gas model and compare with experimental results of vicinage effects in the energy-loss and ionization cross sections for hydrogen molecules interacting with C, Al, Si, Al_2O_3, and SiO_2 targets.

DOI: 10.1103/PhysRevA.99.032702

I. INTRODUCTION

The interaction of swift molecules with solids has been a subject of great interest and activity during the last decades [1–10]. The first experimental evidence of an enhancement of the stopping power of molecular projectiles due to a correlation effect between the particles that compose the molecular projectile, the so-called *vicinage effect*, was observed by Brandt *et al.* [11]. Many experimental [12–27] and theoretical works [1–10,28–30] have been published to date studying different aspects of this phenomenon, such as the influences of the projectile charge, wake effects, elastic collision cascades, molecular explosion, and related effects. Density-functional theory and nonlinear methods for low velocities [2–4] as well as linear methods for intermediate and high energies [5–8,28–30] were developed to calculate the vicinage effect. To characterize this phenomenon, it is useful to define the stopping ratio R as the quotient between the energy loss of the molecular projectiles and the sum of the energy losses of the separated atomic components. One important aspect of the vicinage effect arises from the dependence of the internuclear distance with the dwell time, or in practice, with the target thickness. As R depends on the internuclear distance, for thick targets the average stopping ratio diminishes, since the distances between the particles increase. Another aspect is that for low energies nonlinear phenomena become relevant and, moreover, the projectiles may become neutral and so the charge state effect also becomes important.

Most of the theoretical descriptions of the vicinage effect have been made using the dielectric formulation. This is a natural way to represent the electrodynamical interactions in a dense medium and is particularly useful to consider the interaction with conduction or valence-band electrons. An interesting dielectric model developed in the 1990s by Kaneko [30–33] extends the possibilities of the dielectric approach to evaluate the contributions of inner shells, in this way opening the possibility of more comprehensive stopping power calculations. The so-called wave-packet model (WPM) of Kaneko, based on the use of Gaussian distributions of electrons in momentum space, provides a significant advantage in terms of analyticity, as it yields closed analytical expressions for the dielectric function, with similar properties to those of the Lindhard dielectric model (LDM) corresponding to a free-electron gas [34] but using more appropriate velocity distributions for each atomic shell.

However, one of the restrictions of both LDM and WPM is the absence of energy gaps or binding effects, so that electrons can be excited as free particles and may be detached from the condensed state without spending the minimum energy corresponding to the band gaps in semiconductors or insulators (in the LDM) or the ionization energy in atomic shells (in the WPM). These binding effects have been taken into account in previous approaches [35,36] by introducing a cutoff in the energies into the definition of the dielectric function. In a recent work [37] we developed an extension of the WPM, introducing the energy binding effects into the corresponding dielectric function to evaluate the influence of

*archubi@iafe.uba.ar
†arista@cab.cnea.gov.ar

the energy gap for each shell. The result of this is the so-called extended wave-packet model (EWPM).

In this paper we study the vicinage effects in the interaction of molecular projectiles with solids, considering the effects produced by the excitation of inner shells. For this purpose, we will use two different approaches and will particularly study the stopping ratio and the ionization cross-section ratio at intermediate and high energies. As a case of particular interest we will consider $H_2{}^+$ projectiles with typical internuclear distances to compare with experiments. First we extend the classical electrodynamics atomic-oscillator model (AOM) of Bohr to a semiclassical impact-parameter model (SIPM) for the case of correlated ions. To perform this extension we consider short-distance corrections and screening effects, due to the free electrons in the case of metals or last-shell electrons in the case of insulators and semiconductors, by introducing a Yukawa interaction potential. In addition, we use a quantum-mechanical approach for the bound electrons of the target, keeping the classical representation of the projectile by the impact-parameter method to calculate the ionization cross-section (ICS) ratios. Secondly, we apply the EWPM to calculate the influence of inner-shell contributions to the vicinage effects on the stopping power and the ionization cross-section ratio. Finally, we add the contribution of the valence electrons to the energy loss of correlated ions, using Lindhard's dielectric model [28], and we compare the results of the different models with the experiments.

The present work is organized as follows: In Sec. II we describe the classical model and its semiclassical extension. In Sec. III we develop the quantum-mechanical impact-parameter approach to calculate the ICS ratios and thus complete the semiclassical calculations. In Sec. IV we describe the dielectric approach used in this study and its extension considering the binding energies of the atomic shells. In Sec. V we present the expressions for the energy loss and the ionization cross section. In Sec. VI we show the results of the calculations of the stopping ratios and ionization cross-section ratios for $H_2{}^+$ molecules comparing the SIPM, WPM, and EWPM results with the experiments. The conclusions are summarized in Sec. VII.

II. CLASSICAL AND SEMICLASSICAL DESCRIPTION

To evaluate the contribution of the inner shells to the stopping of bare projectiles by atoms, Bohr proposed a classical electrodynamics model (or atomic-oscillator model). In this model, the bound electrons of the target oscillate with frequency $\omega = \omega_0$, with ω_0 associated to the binding energy of the atomic shell [38–40]. This approach is very useful to calculate the stopping when the projectile passes far apart from the target but has difficulties in representing close interactions [39,40]. Hence, a correction to this model is introduced by considering both classical and quantum-mechanical effects.

Let us consider a pair of ions with charges Z_1e and Z_2e, separated by a distance r_0, moving with velocity v, with trajectories parallel to the z axis. We assume the target atom is fixed at the origin of the coordinate system and define the impact parameters b_1 and b_2 corresponding to the trajectories of each ion (Fig. 1). Considering the position of the target

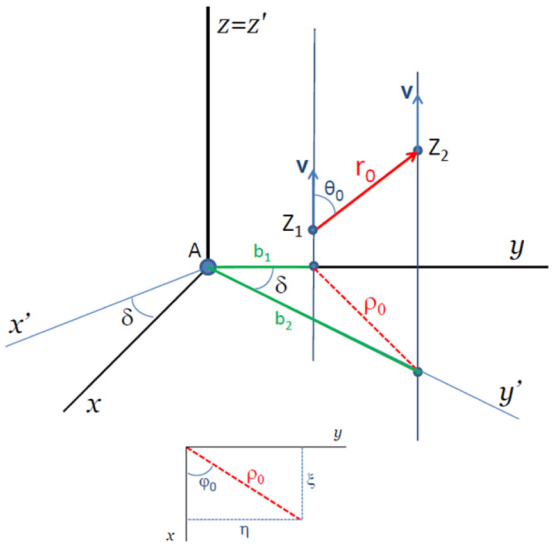

FIG. 1. Diatomic projectile moving along z direction with velocity v and impact parameters b_1 and b_2, respectively. Target is placed at the origin of the coordinate system

atom and the trajectories of each ion, we define a set of axis on the plane perpendicular to z: (x, y) for ion Z_1 and (x', y') for ion Z_2, so that the target atom is at a distance b_1 (along the y axis) with respect to the trajectory of ion Z_1 and at a distance b_2 (along the y' axis) with respect to the trajectory of ion Z_2. Hence, the positions of each ion are given by $(x_1, y_1, z_1) = (0, b_1, vt)$ and $(x_2', y_2', z_2') = (0, b_2, z_0 + vt)$, with $z_0 = r_0\cos(\theta_0)$, where θ_0 and φ_0 are the polar and azimuthal angles of the internuclear vector $\overrightarrow{r}_0$ (Fig. 1). Here $z_1 = vt$ and $z_2 = z_2' = z_0 + vt$ represent the positions of the first and second ion, respectively, along the trajectory axis z.

The time-frequency Fourier transforms of the electric fields produced by each ion on the position of the target atom are given by

$$\begin{Bmatrix} E_z^{(1)}(\omega_0) \\ E_y^{(1)}(\omega_0) \end{Bmatrix} = \frac{Z_1 e}{\sqrt{2\pi}} \int_{-\infty}^{\infty} dt \frac{e^{i\omega_0 t}}{\left[b_1^2 + (vt)^2\right]^{3/2}} \begin{Bmatrix} vt \\ b_1 \end{Bmatrix}, \tag{1}$$

$$\begin{Bmatrix} E_z^{(2)}(\omega_0) \\ E_{y'}^{(2)}(\omega_0) \end{Bmatrix} = \frac{Z_2 e}{\sqrt{2\pi}} \int_{-\infty}^{\infty} dt \frac{e^{i\omega_0 t}}{\left[b_2^2 + (vt + z_0)^2\right]^{3/2}} \begin{Bmatrix} z_0 + vt \\ b_2 \end{Bmatrix}. \tag{2}$$

We note that these are the only no null components of the field of each ion (i.e., the respective x and x' components of ions 1 and 2 are zero).

These integrals can be solved analytically, obtaining

$$\begin{Bmatrix} E_z^{(1)}(\omega_0) \\ E_y^{(1)}(\omega_0) \end{Bmatrix} = \frac{Z_1 e}{\sqrt{2\pi}} \frac{2\omega_0\gamma_1}{v^2} \begin{Bmatrix} iK_0\left(\frac{\omega_0 b_1}{v}\right) \\ K_1\left(\frac{\omega_0 b_1}{v}\right) \end{Bmatrix}, \tag{3}$$

$$\begin{Bmatrix} E_{z'}^{(2)}(\omega_0) \\ E_{y'}^{(2)}(\omega_0) \end{Bmatrix} = \frac{Z_2 e}{\sqrt{2\pi}} \frac{2\omega_0\gamma_2}{v^2} \begin{Bmatrix} iK_0\left(\frac{\omega_0 b_2}{v}\right) \\ K_1\left(\frac{\omega_0 b_2}{v}\right) \end{Bmatrix} e^{-i\omega_0 z_0/v}, \tag{4}$$

where we have introduced a correction factor $\gamma_i = b_i/\sqrt{b_i + (\frac{Z_i}{v^2})^2 + (\frac{1}{2v})^2}$ (in atomic units) to extend the validity of the results to close collisions. The explanation of this

correction factor is based on the discussion given in Ref. [39], considering a classical Rutherford radius $Z_i e^2/mv^2$, and a quantum diffraction-limit parameter $\hbar/2mv$. It may be shown that with this correction the energy loss of each ion (after integrating on impact parameters) agrees well with the Bohr-Bethe-Bloch limit for the stopping power at high velocities, which for this model yields the expression [39]

$$\left|\frac{dE}{dz}\right| = \frac{4\pi n_0 Z^2 e^4}{mv^2}\xi K_0(\xi)K_1(\xi), \tag{5}$$

with $\xi = \omega_0 b_{\min}(v)/v$ and $b_{\min}(v) = \sqrt{(\frac{Z_i}{v^2})^2 + (\frac{1}{2v})^2}$, so that for $\xi \ll 1$, $K_0(\xi) \sim \ln(1.123/\xi)$, $K_1(\xi) \sim 1/\xi$, and the function $\xi K_0(\xi)K_1(\xi)$ reproduces the Bloch behavior for the stopping power in all its limits.

The energy transfer to the bound electron is given, in terms of these fields, by [39]

$$\begin{aligned}\Delta E(b_1, b_2, z_0, v) &= \frac{\pi e^2}{m}|E(\omega_0)|^2 \\ &= \frac{\pi e^2}{m}\left[\left|E_z^{(1)}(\omega_0) + E_z^{(2)}(\omega_0)\right|^2\right. \\ &\quad \left. + \left|\vec{E}_y^{\,(1)}(\omega_0) + \vec{E}_{y'}^{\,(2)}(\omega_0)\right|^2\right].\end{aligned} \tag{6}$$

Notice that the z components of the fields can be summed algebraically since the z and z' axes coincide, while the y and y' components must be summed vectorially since the axes y and y' are not collinear. To evaluate the interference term $\vec{E}_y^{\,(1)} \cdot \vec{E}_{y'}^{\,(2)*}$ we must consider the angle $\delta(\theta_0, \varphi_0)$ between both axes, which is given by (cf. Fig. 1)

$$\delta(\theta_0, \varphi_0) = \arccos\frac{b_1 + \rho_0 \sin(\varphi_0)}{b_2(\theta_0, \varphi_0)}, \tag{7}$$

where $\rho_0 = r_0 \sin(\theta_0)$ is the projection of r_0 on the plane perpendicular to the ion trajectory. Another relevant relation is $b_2(\theta_0, \varphi_0) = \sqrt{\xi^2 + (b_1 + \eta)^2}$, were $\xi = r_0 \sin(\theta_0)\cos(\varphi_0)$ and $\eta = r_0 \sin(\theta_0)\sin(\varphi_0)$ are the x and y components of ρ_0.

The previous expression of ΔE contains the energy loss of two independent ions:

$$\begin{aligned}\Delta E_{\text{indep}} =& \frac{\pi e^2}{m}\left[\left|E_z^{(1)}(\omega_0)\right|^2 + \left|E_y^{(1)}(\omega_0)\right|^2\right. \\ &\left. + \left|E_z^{(2)}(\omega_0)\right|^2 + \left|E_{y'}^{(2)}(\omega_0)\right|^2\right] \end{aligned} \tag{8}$$

$$\begin{aligned}=& \frac{2e^4\omega_0^2}{mv^4}\left\{Z_1^2\gamma_1^2\left[K_0^2\left(\frac{\omega_0 b_1}{v}\right) + K_1^2\left(\frac{\omega_0 b_1}{v}\right)\right]\right. \\ &\left. + Z_2^2\gamma_2^2\left[K_0^2\left(\frac{\omega_0 b_2}{v}\right) + K_1^2\left(\frac{\omega_0 b_2}{v}\right)\right]\right\}\end{aligned} \tag{9}$$

and the interference or vicinage term

$$\begin{aligned}\Delta E_{\text{inter}} =& \frac{\pi e^2}{m} 2\,\text{Re}\left\{E_z^{(1)}(\omega_0)E_z^{(2)*}(\omega_0)\right. \\ &\left. + \vec{E}_y^{\,(1)}(\omega_0) \cdot \vec{E}_{y'}^{\,(2)*}(\omega_0)\right\}\end{aligned} \tag{10}$$

$$\begin{aligned}=& \frac{4e^4\omega_0^2}{mv^4} Z_1 Z_2 \gamma_1 \gamma_2 \left[K_0\left(\frac{\omega_0 b_1}{v}\right)K_0\left(\frac{\omega_0 b_2}{v}\right)\right. \\ &\left. + K_1\left(\frac{\omega_0 b_1}{v}\right)K_1\left(\frac{\omega_0 b_2}{v}\right)\cos(\delta)\right]\cos\left(\frac{\omega_0 z_0}{v}\right).\end{aligned} \tag{11}$$

These results are similar to those obtained by Fadanelli *et al.* [21]. We now assume a random orientation of the internuclear axis r_0. Hence, in order to obtain the stopping power of this cluster we must integrate the energy loss over all the impact parameters b_1 (of projectile Z_1) and over all the possible orientations (θ_0, φ_0) of $\vec{r}_0$. This yields the contribution of a given shell s in the form

$$\begin{aligned}\frac{dE^{(s)}}{dz} =& 2\pi n_a N_e^{(s)} \int_0^\infty b_1 db_1 \int_0^\pi \int_0^{2\pi} \Delta E(b_1, b_2, z_0, v) \\ &\times G(b_1, b_2)\sin(\theta_0) d\theta_0 d\varphi_0,\end{aligned} \tag{12}$$

where n_a is the atomic density and $N_e^{(s)}$ is the number of electrons in the considered shell. Notice that in this integral the impact parameter b_2 must be considered a function θ_0 and φ_0, according to the function $b_2(\theta_0, \varphi_0)$ given before. Additionally, to test possible *localization effects* we have introduced here a function $G(b_1, b_2)$ that will be used to make a detailed analysis of the contributions of close and distant collisions, as described in Sec. VI.

A. Screening effects

The previous expressions consider the electric fields of particles moving in vacuum. One important aspect that was not taken into account so far is the effect of the surrounding medium, i.e., the screening effect produced by the rest of the electrons. To account for this effect we replace the previous Coulomb interaction by a Yukawa potential, namely,

$$\phi(\vec{r}, t) = Z_1 e\frac{e^{-\alpha r_1(t)}}{r_1(t)} + Z_2 e\frac{e^{-\alpha r_1(t)}}{r_1(t)}, \tag{13}$$

where $r_1(t) = \sqrt{b_1^2 + (vt)^2}$, $r_2(t) = \sqrt{b_2^2 + (vt + z_0)^2}$. Taking the gradient of this potential, we obtain the electric field and then calculate the corresponding Fourier components by the integrals

$$\begin{aligned}\begin{Bmatrix}E_z^{(1)}(\omega_0)\\ E_y^{(1)}(\omega_0)\end{Bmatrix} =& \frac{Z_1 e}{\sqrt{2\pi}}\int_{-\infty}^{\infty} dt\,\frac{[1 + \alpha r_1(t)]}{r_1(t)^3} \\ &\times e^{i\omega_0 t}e^{-\alpha r_1(t)} \times \begin{Bmatrix}vt\\ b_1\end{Bmatrix},\end{aligned} \tag{14}$$

$$\begin{aligned}\begin{Bmatrix}E_z^{(2)}(\omega_0)\\ E_{y'}^{(2)}(\omega_0)\end{Bmatrix} =& \frac{Z_2 e}{\sqrt{2\pi}}\int_{-\infty}^{\infty} dt\,\frac{[1 + \alpha r_2(t)]}{r_2(t)^3} \\ &\times e^{i\omega_0 t}e^{-\alpha r_2(t)} \times \begin{Bmatrix}z_0 + vt\\ b_2\end{Bmatrix}.\end{aligned} \tag{15}$$

Incidentally, these integrals may also be evaluated analytically as shown in [41]. In this case we obtain the results

$$E_z^{(1)}(\omega_0) = \frac{Z_1 e}{\sqrt{2\pi}}\frac{2i\omega_0\gamma_1}{v^2}K_0\left(\frac{\omega_1 b_1}{v}\right), \tag{16}$$

$$E_y^{(1)}(\omega_0) = \frac{Z_1 e}{\sqrt{2\pi}}\frac{2\omega_1\gamma_1}{v^2}K_1\left(\frac{\omega_1 b_1}{v}\right), \tag{17}$$

$$E_z^{(2)}(\omega_0) = \frac{Z_2 e}{\sqrt{2\pi}}\frac{2i\omega_0\gamma_2}{v^2}K_0\left(\frac{\omega_1 b_2}{v}\right)e^{-i\omega_0 z_0/v}, \tag{18}$$

$$E_{y'}^{(2)}(\omega_0) = \frac{Z_2 e}{\sqrt{2\pi}} \frac{2\omega_1 \gamma_2}{v^2} K_1\left(\frac{\omega_1 b_2}{v}\right) e^{-i\omega_0 z_0/v}, \quad (19)$$

where $\omega_1 = \sqrt{\omega_0^2 + \alpha^2 v^2}$ and where the Bloch correction factors γ_i have also been included following the considerations of the previous section. In the following applications we use the dynamical screening approximation [42], $\alpha = \omega_p/v$, where ω_p is the plasma frequency, so that $\omega_1 = \sqrt{\omega_0^2 + \omega_p^2}$, which corresponds to the characteristic frequency of bound electrons in dense media [43].

The rest of the calculations follow the lines of the previous ones, integrating over impact parameters and angular variables as in Eq. (12) to obtain the stopping power values. The corresponding *stopping ratios* are given by the quotient between the stopping of the correlated protons and the stopping of two independent protons, and provide the information on the vicinage effects.

III. QUANTUM IMPACT-PARAMETER METHOD

The previous calculations may be complemented by a more comprehensive semiclassical description where the projectiles keep the classical trajectory properties while the atomic electrons are treated in quantum-mechanical terms. In this case, the probability of transition from an initial state $|i\rangle$ to a final state $|f\rangle$ may be calculated by first-order perturbation theory as $P_{\rm tot} = |a_{\rm if}|^2$, where the amplitude $a_{\rm if}$ is given by [44]

$$a_{\rm if} = \frac{1}{i\hbar}\int_{-\infty}^{\infty} e^{i\omega t}\langle f|V(\vec{r},t)|i\rangle dt \quad (20)$$

and where $V(\vec{r},t)$ is the interaction potential.

We consider first the case of particles interacting in vacuum and include the screening effects later on. So in this first case the interaction potential is

$$V_0(\vec{r},t) = \frac{-Z_1 e^2}{|\vec{r} - \vec{r}_1(t)|} + \frac{-Z_2 e^2}{|\vec{r} - \vec{r}_2(t)|}, \quad (21)$$

where $\vec{r}_1(t)$ and $\vec{r}_2(t)$ are the corresponding trajectories of both ions.

To make contact with the previous formulation, we now expand this potential around the position of the target atom up to dipole-order dipole terms,

$$V_0(\vec{r},t) \cong \sum_i \left[\frac{-Z_i e^2}{|\vec{r}_i(t)|} + \frac{Z_i e^2}{|\vec{r}_i(t)|^3}\vec{r}\cdot\vec{r}_i(t)\right] = V_0(0,t) + e\vec{E}(0,t)\cdot\vec{r}, \quad (22)$$

and replacing this in Eq. (20) we obtain

$$a_{\rm if} = \sqrt{2\pi}\frac{e}{i\hbar}\vec{E}(\omega_0)\cdot\langle f|\vec{r}|i\rangle. \quad (23)$$

Considering the three components of $\langle f|\vec{r}|i\rangle$ with $\vec{r} = (x,y,z)$, between initial $|i\rangle = |0\rangle$ and final states $|f\rangle$ [notation: $(x)_{f0}$, $(y)_{f0}$, $(z)_{f0}$] and the expressions for the electric field, Eqs. (1)–(4), we get the corresponding terms (notice that we must also include here the x component of the electric field generated by the ion Z_2, which is calculated in a similar way to the other components):

$$a_f^{(x)} = (x)_{f0}\frac{2e^2\omega_0 Z_2\gamma_2}{i\hbar v^2}\left[K_1\left(\frac{\omega_0 b_2}{v}\right)e^{-i\omega_0 z_0/v}\sin(\delta)\right], \quad (24)$$

$$a_f^{(y)} = (y)_{f0}\frac{2e^2\omega_0}{i\hbar v^2}\left[Z_1\gamma_1 K_1\left(\frac{\omega_0 b_1}{v}\right) + Z_2\gamma_2 K_1\left(\frac{\omega_0 b_2}{v}\right)e^{-i\omega_0 z_0/v}\cos(\delta)\right], \quad (25)$$

$$a_f^{(z)} = (z)_{f0}\frac{2e^2\omega_0}{\hbar v^2}\left[Z_1\gamma_1 K_0\left(\frac{\omega_0 b_1}{v}\right) + Z_2\gamma_2 K_0\left(\frac{\omega_0 b_2}{v}\right)e^{-i\omega_0 z_0/v}\right], \quad (26)$$

and considering also conditions of isotropy of the initial state [44], so that $|(x)_{f0}|^2 = |(y)_{f0}|^2 = |(z)_{f0}|^2$, the total transition probability takes the form

$$P_{\rm tot} = P_{\rm ind} + P_{\rm vic}, \quad (27)$$

where $P_{\rm ind}$ and $P_{\rm vic}$ represent the transition probabilities for independent ions and the vicinage term, respectively, given by

$$P_{\rm ind}(b_1,b_2) = \left(\frac{2e^2\omega_0}{\hbar v^2}\right)^2 |(x)_{f0}|^2\left\{Z_1^2\gamma_1^2\left[K_0^2\left(\frac{\omega_0 b_1}{v}\right) + K_1^2\left(\frac{\omega_0 b_1}{v}\right)\right] + Z_2^2\gamma_2^2\left[K_0^2\left(\frac{\omega_0 b_2}{v}\right) + K_1^2\left(\frac{\omega_0 b_2}{v}\right)\right]\right\}, \quad (28)$$

$$P_{\rm vic}(b_1,b_2) = 2Z_1Z_2\left(\frac{2e^2\omega_0}{\hbar v^2}\right)^2 |(x)_{f0}|^2\gamma_1\gamma_2\cos\left(\frac{\omega_0 z_0}{v}\right)\left[K_0\left(\frac{\omega_0 b_1}{v}\right)K_0\left(\frac{\omega_0 b_2}{v}\right) + K_1\left(\frac{\omega_0 b_1}{v}\right)K_1\left(\frac{\omega_0 b_2}{v}\right)\cos(\delta)\right], \quad (29)$$

δ being the angle between the axes y and y'.

We may now perform an angular average of these terms, considering a random distribution of the internuclear axis orientation $\vec{r}_0$ by the integral

$$\overline{P_{\rm tot}}(b_1) = \frac{1}{4\pi}\int_0^{2\pi} d\phi_0 \int_0^{\pi} P_{\rm tot}(b_1,b_2)\sin(\theta_0)d\theta_0, \quad (30)$$

with the following internal relations: $z_0 = r_0\cos(\theta_0)$, $\rho_0 = r_0\sin(\theta_0)$, $b_2(\theta_0,\varphi_0) = \sqrt{\xi^2 + (b_1+\eta)^2}$, where $\xi = r_0\sin(\theta_0)\cos(\varphi_0)$ and $\eta = r_0\sin(\theta_0)\sin(\varphi_0)$, and the angle $\delta = \delta(\theta_0,\varphi_0)$ given by Eq. (7). Finally, the inelastic mean-free path (IMFP) and related cross section are obtained by integrating over the remaining free parameter b_1:

$$\frac{1}{\lambda} = n_0\sigma = 2\pi n_0\int \overline{P_{\rm tot}}(b_1)b_1 db_1. \quad (31)$$

It is of interest to show here a relationship between the inverse mean-free path $1/\lambda$ and the stopping power derived

earlier. For the sake of simplicity, we will consider only the case of a single ion so that the excitation probability reduces to

$$P(b) = \left(\frac{2e^2\omega_0}{\hbar v^2}\right)^2 |(x)_{f0}|^2 Z^2\gamma^2\left[K_0^2\left(\frac{\omega_0 b}{v}\right) + K_1^2\left(\frac{\omega_0 b}{v}\right)\right]. \tag{32}$$

The integral over b_1 may be performed analytically using the well-known result [39]

$$\int_{b_{\min}}^{\infty}\left[K_0^2\left(\frac{\omega_0 b}{v}\right) + K_1^2\left(\frac{\omega_0 b}{v}\right)\right] b db = \left(\frac{v}{\omega_0}\right)^2 \xi K_0(\xi)K_1(\xi), \tag{33}$$

with $\xi = \omega_0 b_{\min}/v$. The parameter $b_{\min}$ represents here the required correction to avoid the divergence of the Coulomb interaction at very short distances so that the correction factor γ here is no longer necessary. Hence, the IMFP becomes

$$\frac{1}{\lambda} = \frac{8\pi n_0 Z^2 e^4}{\hbar^2 v^2}|(x)_{f0}|^2 \xi K_0(\xi)K_1(\xi). \tag{34}$$

We recall now the definition of the dipole oscillator strength [44],

$$F_{\rm fi} = \frac{2m}{\hbar^2}\Delta E_{\rm fi}\,|(x)_{\rm fi}|^2, \tag{35}$$

so that Eq. (34) may be written in the form

$$\frac{\Delta E_{\rm fi}}{\lambda} = \frac{4\pi Z^2 e^4}{m v^2} F_{\rm fi} n_0\, \xi K_0(\xi)K_1(\xi), \tag{36}$$

which shows a nice agreement with the corresponding expression for the stopping power, Eq. (5), provided that we identify the factor $n_{\rm eff} = F_{\rm fi} n_0$ as the effective electron density according to a classical picture of the interaction (and consistent with the total oscillator strength sum rule: $\sum_f F_{\rm fi} = Z_t$).

Finally, we must consider the screening effects, which may be important in the case of solid targets. Using the results of the screened fields, Eqs. (16)– (19), we obtain the expressions for the probability terms $P_{\rm ind}^{\rm screen}$ and $P_{\rm vic}^{\rm screen}$ for inner-shell excitation in a screening medium as follows:

$$P_{\rm ind}^{\rm screen}(b_1,b_2) = \left(\frac{2e^2\omega_0}{\hbar v^2}\right)^2 |(x)_{f0}|^2 \left\{Z_1^2\gamma_1^2\left[K_0^2\left(\frac{\omega_1 b_1}{v}\right) + \left(\frac{\omega_1}{\omega_0}\right)^2 K_1^2\left(\frac{\omega_1 b_1}{v}\right)\right] + Z_2^2\gamma_2^2\left[K_0^2\left(\frac{\omega_1 b_2}{v}\right) + \left(\frac{\omega_1}{\omega_0}\right)^2 K_1^2\left(\frac{\omega_1 b_2}{v}\right)\right]\right\}, \tag{37}$$

$$P_{\rm vic}^{\rm screen}(b_1,b_2) = 2Z_1Z_2\left(\frac{2e^2\omega_0}{\hbar v^2}\right)^2 |(x)_{f0}|^2 \gamma_1\gamma_2 \cos\left(\frac{\omega_0 z_0}{v}\right)\left[K_0\left(\frac{\omega_1 b_1}{v}\right)K_0\left(\frac{\omega_1 b_2}{v}\right) + \left(\frac{\omega_1}{\omega_0}\right)^2 K_1\left(\frac{\omega_1 b_1}{v}\right)K_1\left(\frac{\omega_1 b_2}{v}\right)\cos(\delta)\right]. \tag{38}$$

The corresponding angular averages are given by Eq. (30), and the final average over impact parameters are calculated as in Eq. (31).

IV. KANEKO'S WAVE-PACKET MODEL

The main assumption of this model is the consideration of Gaussian distributions for the electron velocities of a given atomic shell, i.e., $f(v) \sim e^{-v^2/\overline{v}^2}$, where $\overline{v}$ is a characteristic speed of the considered shell. The dielectric function for these systems is described in terms of a characteristic wave vector $\overline{q}$, which is related to $\overline{v}$ by $\hbar\overline{q} = m_e\overline{v}$. The value of $\overline{q}$ is determined by the relation $\overline{q} = q_1 N^{1/3}$, where N is the number of electrons in the shell and q_1 is a shell parameter whose value is determined from Hartree-Fock calculations of electron velocity distributions using the results of previous authors [45,46].

A. Dielectric function

The wave-packet model yields closed analytical expressions for the real and imaginary parts of the dielectric function $\epsilon(k,\omega) = \epsilon_1(k,\omega) + i\epsilon_2(k,\omega)$, where k and ω are the wave-vector and frequency variables. The results for ϵ_1 and ϵ_2 may be cast in a convenient way in terms of the dimensionless variables $u = \omega/k\overline{v}$ and $z = k/2\overline{q}$ as follows [31]:

$$\epsilon_1(u,z) = 1 + \frac{\chi^2}{z^2}\frac{1}{8z}[F(u+z) - F(u-z)], \tag{39}$$

$$\epsilon_2(u,z) = \frac{\chi^2}{z^2}\frac{\pi}{8z}\left[e^{-(u-z)^2} - e^{-(u+z)^2}\right], \tag{40}$$

where the parameter $\chi^2 = e^2/\pi\hbar\overline{v}$.

The function $F(x)$ is defined by

$$F(x) = \sqrt{\pi}\Psi(x) = \sqrt{\pi}\int_0^{\infty}\sin(tx)e^{-t^2/4}dt. \tag{41}$$

An alternative expression for $\Psi(x)$ (more useful for numerical calculations) is

$$\Psi(x) = \frac{\varphi(\sqrt{2}x)}{x} \tag{42}$$

where

$$\varphi(x) = x\int_0^x e^{(t^2-x^2)/2}dt\,. \tag{43}$$

B. Extended wave-packet model

As indicated before, one of the restrictions of the WPM is the absence of energy gaps or binding effects, so that electrons can be excited as if they were free particles and easily removed from the atomic shells. In a recent work we extended the WPM, introducing energy binding corrections in the dielectric function, making use of a general method proposed by Levine and Louie [35]. In our EWPM [37] the new dielectric function $\widetilde{\epsilon}$ becomes, for $\omega > \omega_0$,

$$\widetilde{\epsilon}_1(k,\omega) = \epsilon_1\left(k, \sqrt{\omega^2 - \omega_0^2}\right), \tag{44}$$

$$\widetilde{\epsilon}_2(k,\omega) = \epsilon_2\big(k, \sqrt{\omega^2 - \omega_0^2}\big), \tag{45}$$

whereas for $\omega < \omega_0$, $\widetilde{\epsilon}_2(k,\omega) = 0$, while $\widetilde{\epsilon}_1(k,\omega)$ is obtained from $\widetilde{\epsilon}_2(k,\omega)$ using the Kramers-Kronig relations. All the quantities calculated here are obtained from integrals in the domain $\omega > \omega_0$, where the values of $\widetilde{\epsilon}_1$ and $\widetilde{\epsilon}_2$ can be expressed analytically in terms of Eqs. (39)–(45). This dielectric function also satisfies the sum rules as it does the Lindhard dielectric function for a free-electron gas.

V. IONIZATION CROSS-SECTION AND STOPPING RATIOS

We are here interested in calculating the first two moments of the energy-loss distribution for $H_2{}^+$ projectiles traversing the foil in a random orientation. Applying the formalism developed in [1,28] to each inner shell of the target atom, we obtain the integrals (with $n = 0, 1$)

$$Q_n = \frac{2}{\pi}\left(\frac{e}{v}\right)^2 \hbar^{n-1} \int_0^\infty \frac{dk}{k} \int_0^{kv} \omega^n d\omega \, \mathrm{Im}\left[\frac{-1}{\widetilde{\epsilon}(k,\omega)}\right] \times \left[\left(Z_1^2 + Z_2^2\right) + f(k) 2Z_1Z_2 \frac{\sin(kr)}{kr}\right], \tag{46}$$

where $Z_i = 1$ are the atomic numbers of the incident nucleons and v is the molecular projectile velocity. This formula is similar to the expression obtained in Ref. [28] for a free-electron gas model (FEG) where the interference contribution is given by $I(r) = 2Z_1Z_2 \sin(kr)/kr$. However, we have introduced here the EWPM dielectric function corresponding to the target specific inner shell. We also add a "localization effect" through the Gaussian "cutoff" function $f(k) = e^{-\alpha \frac{k^2}{<v^2>}}$ centered in zero and defined in terms of the average square velocity of that shell. This form of cutoff function was introduced by Kihara and Aono [47] as a method to separate short-range and long-range collisions. In our case, for molecules, the purpose of this function is to softly reduce a possible overestimation of the interference contribution for very close collisions of both protons (a low-probability event as shown in Fig. 2). In fact, the results of the calculations for the different targets showed negligible differences for all the atomic levels in the values of the interference term when this function was used, with the standard value $\alpha = 1.5$ and with the respective values of the square velocities. This agrees with the results of SIPM calculations in Fig. 2, which shows negligible contribution from the close-close interference terms.

This expression of Q_n yields the values of the inverse inelastic mean-free path and stopping power when $n = 0, 1$, namely,

(i) inverse inelastic mean-free path: $1/\lambda_i = Q_0$

(ii) stopping power: $S = |\langle dE/dx \rangle| = Q_1$

Another quantity of interest is the ionization cross section, which is directly related to the IMFP λ_i by

$$\sigma_i = \frac{1}{n_a \lambda_i}, \tag{47}$$

where n_a is the atomic density.

The stopping and ionization cross-section ratios are given by the quotient $Q_n/2Q_n^{(p)}$, where $Q_n^{(p)}$ is the ionization cross section ($n = 0$) or the stopping ($n = 1$) of a bare proton. Several examples of calculations for specific cases will be considered in the next section.

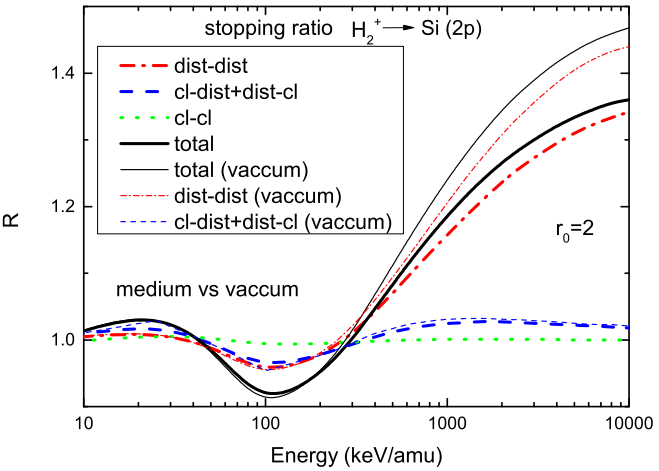

FIG. 2. Stopping ratio of $H_2{}^+$ in a Si target as a function of the projectile energy, separated contributions from the $2p$ shell for distant and close collisions.

VI. CALCULATIONS

A. Stopping power ratios

As a measure of the vicinage effect, we consider here the average stopping power ratio $\overline{R}$, calculated as

$$\overline{R} = \frac{\overline{\Delta E}_{\mathrm{cluster}}}{\overline{\Delta E}_{\mathrm{indep}}} = 1 + \frac{\overline{\Delta E}_{\mathrm{inter}}}{\overline{\Delta E}_{\mathrm{indep}}}, \tag{48}$$

where $\overline{\Delta E}_{\mathrm{indep}}$ and $\overline{\Delta E}_{\mathrm{inter}}$ are the complete angular and impact-parameter averages of the stopping terms corresponding to independent ions ($\overline{\Delta E}_{\mathrm{indep}}$) and the associated interference term ($\overline{\Delta E}_{\mathrm{inter}}$), respectively, and $\overline{\Delta E}_{\mathrm{cluster}}$ is the total stopping power average for the group of ions.

In Fig. 2 we perform a study of close and distant collisions, with the SIPM separating those collisions with impact parameters lower than the average radium a_{2p} corresponding to the atomic $2p$ shell (with $a_{2p} = 0.535$ for the case of Si [48]) from those collisions with impact parameters larger than a_{2p}. Here we have separated the different cases considering (a) that both nucleons traverse the $2p$ electronic cloud (close-close), (b) one of the nucleons crosses the $2p$ cloud while the other passes outside it (close-distant and distant-close), and (c) both nucleons pass outside the $2p$ cloud (distant-distant). To perform this analysis we make use of the $G(b_1, b_2)$ function in Eq. (12), considering (a) $G(b_1, b_2) = 1$ if both b_1 and b_2 are less than a_{2p}, and 0 otherwise; (b) $G(b_1, b_2) = 1$ if one of the b_i is less than a_{2p} while the other is larger, and 0 otherwise; and (c) $G(b_1, b_2) = 1$ if both b_1 and b_2 are larger than a_{2p}, and 0 otherwise. We observe that the relative contribution to the interference ratio from very close collisions (close-close) is almost negligible. The contribution from distant-distant collisions is similar to the contribution from close-distant collisions at intermediate energies (~100 keV), probably due to the fact that the projectile energy is relatively low and requires close collisions to excite that shell. For higher energies the

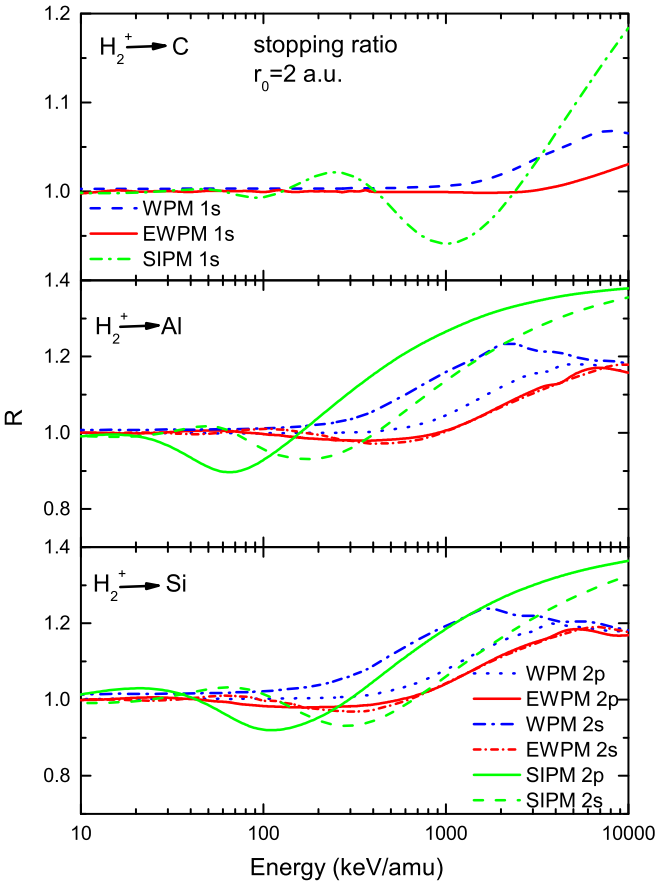

FIG. 3. Separated contributions from inner shells to the stopping ratio calculated with three different theoretical models: SIPM, WPM, and EWPM. The results are displayed for H_2^+ projectiles in C, Al and Si targets as a function of the projectile energy.

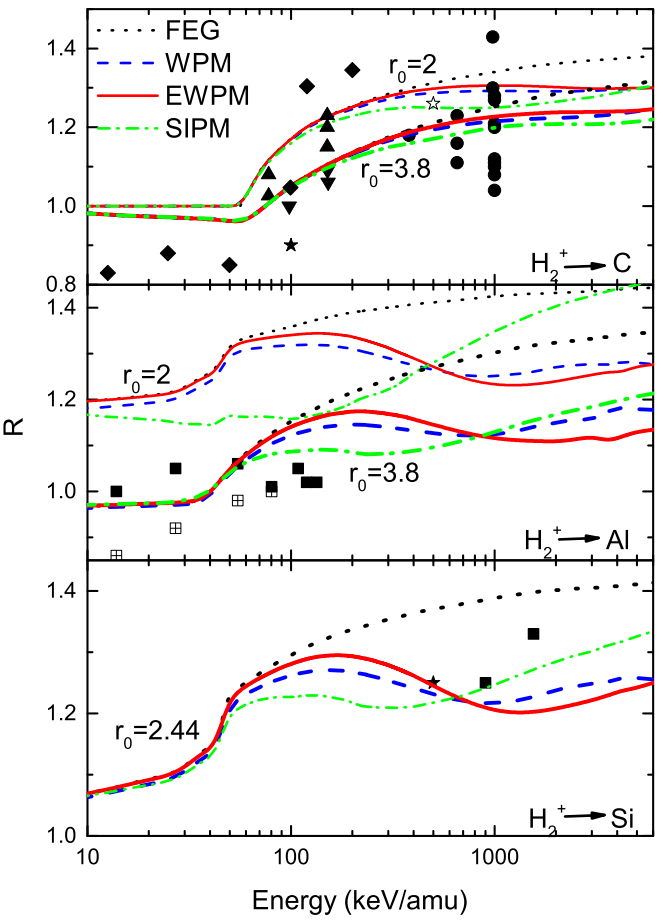

FIG. 4. FEG and total contributions to the stopping ratio for H_2^+ in C, Al, and Si targets as a function of the projectile energy for three different models: SIPM, WPM, and EWPM. Experimental results: circles, Tape *et al.* [12]; triangles, squares, Eckardt *et al.* [13]; inverted triangles, Nyaiesh *et al.* [14]; full stars, Horino [15]; open stars, Matsunami [19]; open triangles, Touchrift *et al.* [20]; diamonds, Koval *et al.* [4].

contribution from distant collisions becomes dominant. The same figure also shows the effect of screening produced by the electrons of the target. This effect becomes important for distant collisions, reducing its contribution to the stopping ratio, as it is observed comparing the respective results (medium vs vacuum).

In Fig. 3 we analyze the contribution of the most relevant inner shells to the stopping ratio for a pair of correlated protons traversing three different elements: (a) C, (b) Al, and (c) Si. We include here WPM, EWPM, and SIPM calculations for a typical value of the internuclear distance r_0. The strong oscillatory behavior displayed by the SIPM results at lower energies is a consequence of the oscillatory factor $\exp(-i\omega_0 z_0/v)$ in the interference between the fields of both particles; the physical origin of this factor is the time delay in the interaction of both ions with the same target atom. By contrast, this oscillatory effect is not observed in the WPM and EWPM representations, since in these cases the interactions are fully delocalized (the position of the target atom is undefined), and so the phase factor is replaced by the angular average $\sin(kr)/kr$ [28], which produces much weaker oscillations. This behavior almost disappears for the EWPM model. Finally, the comparison between the WPM and EWPM approaches shows that the binding energy effect produces a significant reduction of the interference effect originally calculated with the WPM model for all the shells.

Figure 4 shows Lindhard's FEG and the total stopping ratios for the same C, Al, and Si targets, together with several experimental results. Calculations for significant values of the internuclear distance r_0 are displayed, in the range of 2–3.8 a.u., pertaining to the case of correlated protons with increasing internuclear distances as they travel through a foil. The typical range of experimental distances considered by Brandt starts from an initial spread distribution at around $r_0 = 2.44$ a.u. and increases as the protons move through the target foil [11], while Eckardt *et al.* [13] estimated that, for H_2 molecules traversing an Al target, the average internuclear distances in the foil should be in the range 3 a.u. $< r_0 <$ 5 a.u. Our theoretical results with fixed internuclear distances provide a rough estimation of the experiments, since the internuclear distance increases as the ions move along the trajectory due to several physical factors, such as electrostatic repulsion and multiple scattering of the ions with the target atoms, as well as interactions with the target electrons. The

behavior of the curves seems to follow the asymptotic trend of the experimental values. For C targets, the experiments show a negative vicinage effect ($R < 1$) at low energies which is not reproduced by our calculations. Moreover, there is a very wide spread of experimental values at larger energies so that no precise comparisons can be made. A distinct behavior is observed for Al targets, where the experiments suggest a range of distances of the order of 3.8 a.u. Unfortunately, no experimental data is available for higher energies where the theoretical results increase and split more significantly. At very low energies possible charge effects and nonlinear effects neglected by our theoretical calculations may cause visible discrepancies with experimental results. On the other hand, for a Si target WPM, EWPM, and SIPM results shows reasonable estimations of the interference contribution considering an internuclear distance in accord with Brandt's assumption. Here SIPM seems to better reproduce the trend to higher energies, but again, the lack of experiments in this range precludes more conclusive comparisons.

Still further evidences of vicinage effects for dicluster ions have been obtained more recently from energy-loss experiments on Al_2O_3 and SiO_2 [4,26]. Here we can extend our theoretical description to these compound materials, separating the valence and inner-shell contributions in the following way. The excitation of valence electrons can be conveniently modeled by an electron gas with an effective r_s value and with an energy gap E_g. From experiments of plasmon excitation, both materials exhibit plasmon peaks with very similar energies of nearly 25 eV [49], corresponding to $r_s = 1.56$, while the energy gap for these materials is about 8 eV in both cases [50]. Formation of these valence bands involves 18 outer electrons in Al_2O_3 and 12 electrons in SiO_2. Hence, the residual inner shells involve the $1s$, $2s$, and $2p$ shells of Al and Si, and the $1s$ and $2s$ shells of O. Assuming that the inner shells maintain basically their atomic character, we can calculate the corresponding stopping power by making use of the Bragg rule, which for a molecule with structure A_mB_n is given by [51]

$$\triangle E^{\text{Bragg}}(A_mB_n) = m\triangle E(A) + n\triangle E(B) \tag{49}$$

and so the total energy loss of each compound is finally obtained as

$$\triangle E = \triangle E_{\text{IS}}^{\text{Bragg}} + \triangle E_{\text{val}(r_s,E_g)}, \tag{50}$$

where $\triangle E_{\text{IS}}^{\text{Bragg}}$ and $\triangle E_{\text{val}(r_s,E_g)}$ are the energy losses corresponding to the excitation of inner shells and valence electrons, respectively.

In Fig. 5 we show the existing experimental results from [4,26] together with our model calculations. Here the experiments show (as in the case of C) a distinct behavior at low energies, with negative vicinage effects (i.e., $R < 1$). Our theoretical calculations cannot reproduce this behavior. In a more recent work [52] this particular effect was quantitatively explained by a more sophisticated set of calculations that considered nonlinear effects in screening and energy transfer by a dicluster ion. On the other hand, the behavior at larger energies shows first a rapid growth followed by a more moderate behavior. In this range of energies, our calculations approach the experimental results. We also notice that the

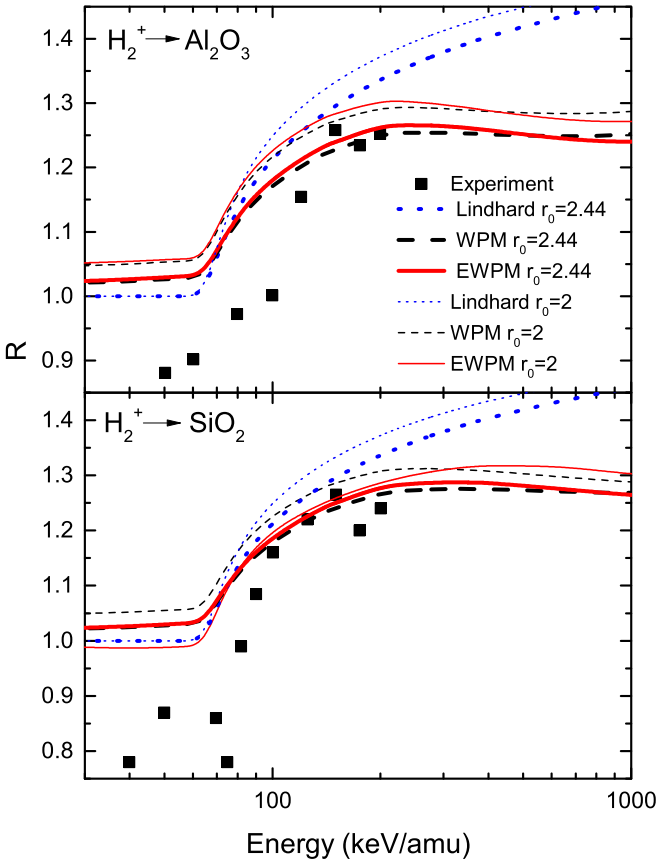

FIG. 5. FEG and total contributions to the stopping ratio for H_2^+ in Al_2O_3 and SiO_2 targets as a function of the projectile energy for two different models: WPM and EWPM. Experimental results: squares, Koval *et al.* [4] for Al_2O_3 and Shubeita *et al.* [26] for SiO_2.

pure-electron-gas calculations (indicated as Lindhard in the figure), which do not consider inner shells, show a continuous growth of R which could not be correct. Moreover, as in the case of simple elements (Fig. 4), the question arises as to what the behavior of R for larger energies should be. Our calculations predict a declining effect. This is a subject open to further experimental research.

Finally, as it was just noted, the theoretical results considering the contribution of inner shells produce a visible lowering of the stopping ratios for higher energies with respect to those calculated for a FEG. This is particularly clear for Al and Si in Fig. 4 and for the two oxides in Fig. 5. The reason for this effect is that the stopping ratio contains a combination of independent and interference terms of the form

$$\overline{R} = 1 + \frac{\overline{\Delta E}_{\text{inter}}^{\text{FEG}} + \overline{\Delta E}_{\text{inter}}^{\text{IS}}}{\overline{\Delta E}_{\text{indep}}^{\text{FEG}} + \overline{\Delta E}_{\text{indep}}^{\text{IS}}}, \tag{51}$$

where the upper scripts FEG and IS indicate the contributions of the FEG and inner shells, respectively. So, when the energy threshold for inner-shell contributions is overpassed, the terms $\overline{\Delta E}_{\text{indep}}^{\text{IS}}$ in the denominator exhibit fast growth [53] while the corresponding interference terms $\overline{\Delta E}_{\text{inter}}^{\text{IS}}$ have a more

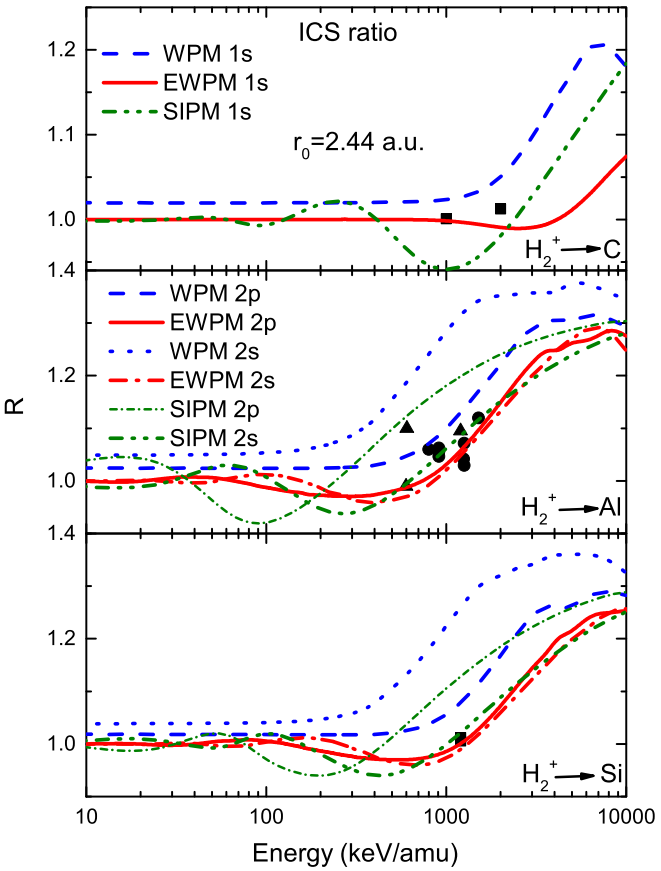

FIG. 6. Inner-shell contributions to the ionization ratio calculated with three different theoretical models: SIPM, WPM, and EWPM. The results are displayed for H_2^+ projectiles in C, Al, and Si targets as a function of the projectile energy. Experimental results: squares, K shell for C and L shell for Si by Lurio and Andersen [22]; circles, L shell by Ootuka *et al.* [23,24]; triangles, L shell by Yamazaki *et al.* [25].

moderate behavior. The consequence of this is a drop in the $\overline{R}$ values as compared with those of a plain electron gas.

B. Inverse mean-free path and ionization cross-section ratios

The vicinage effect in this case is represented by a ratio $\overline{R}$ defined in a similar way as in the stopping power case [Eq. (48)], replacing the terms $\overline{\Delta E}_{\rm indep}$ and $\overline{\Delta E}_{\rm inter}$ by the probability terms $\overline{P}_{\rm ind}$ and $\overline{P}_{\rm vic}$, which are obtained from the average of the terms $P_{\rm ind}(b_1, b_2)$ and $P_{\rm vic}(b_1, b_2)$ defined before.

As a final test of EWPM and SIPM we consider now the calculation of inelastic cross sections. These quantities are highly sensitive to energy binding effects; therefore, these calculations provide a very stringent numerical test to the present approach. Figure 6 shows the results for C, Al, and Si ionization cross-section ratios together with some experimental results for the relevant inner shells using the typical value proposed by Brandt *et al.* [11] for the internuclear distance. A significant improvement of the theoretical results introducing the binding energy with the EWPM model is observed for Si and Al targets, as for the case of protons [37]. For the C target, the results are not conclusive. On the other hand, SIPM results for Si and Al targets show a strong difference between $2p$ and $2s$ shells. However, experiments show very few points for all the targets and do not distinguish between $2s$ and $2p$ shells. Thus more experiments should be performed to test the effects predicted by our calculations; in particular, the expected growth of the vicinage effects in the L-shell ionization of Al and Si for energies over 2 MeV/u, as shown in Fig. 6.

VII. CONCLUSIONS

In this work we have studied the vicinage effects in the energy loss of pairs of correlated protons corresponding to the incidence of swift H_2^+ ions on solid targets. We considered two alternative methods: a semiclassical description and the dielectric approach. One one side, we have reformulated the semiclassical impact-parameter method (SIPM), taking into account screening and close-collision corrections, and on the other, we have used a recently extended wave-packet model (EWPM) that includes the effect of energy thresholds on a dielectric formulation based on Gaussian wave packets in order to describe inner-shell excitations.

The dielectric formulation for the energy loss of correlated ions is good for delocalized excitations, such as in the case of valence or conduction electrons. However, it is not quite appropriate to describe correlated excitations of inner-shell electrons, since it does not take properly into account the localization effects associated with different impact parameters of the moving ions with respect to a target atom. For this reason, the semiclassical description based on the impact-parameter method (SIPM), as reformulated here, provides a more adequate representation. As a test of both methods, we have performed specific calculations of vicinage effects in energy losses and inner-shell ionization for various accessible targets (C, Al, Si, Al_2O_3, and SiO_2) and compared the calculations with existing experimental results. In particular, we described the important effects produced by the screening, the role of close and distant collisions, and the effects of energy thresholds. Inclusions of close-collision corrections (both from classical and quantum origin) and screening effects produce significant improvements on the impact-parameter representation and provide more adequate results than when those effects are neglected.

Some of the important aspects of the phenomenon studied here are the following:

(1) The relative contribution of close and distant collisions was studied using the SIPM approach, showing the growing importance of distant collisions in the vicinage effect with increasing energies, both in stopping power and inner-shell excitations.

(2) The screening of the interactions reduces the magnitude of the vicinage effects, because it reduces the contribution of distant collisions according to the description provided by the SIPM method.

(3) The onset of inner-shell excitations produces an additional decrease in the vicinage effect, because the stopping terms corresponding to inner-shell excitations by independent ions grow more drastically than the corresponding interference terms. The effect arising from these calculations has not been experimentally observed so far. Experimental verification of this prediction would require higher energies than those so far explored.

(4) Existing experimental data on stopping as well as inner-shell excitations have covered so far mainly the low and intermediate energy ranges, where the effects are not so strong, and show in some cases very large dispersion of results (like the case of *C*).

The present work strongly suggests new experiments at intermediate and higher energies to test new theoretical predictions and revealing differences between various models.

ACKNOWLEDGMENTS

This work was supported by the following institutions of Argentina: Consejo Nacional de Investigaciones Científicas y Técnicas, Agencia Nacional de Promoción Científica y Tecnológica, and Universidad de Buenos Aires. We are grateful to Dr. Pedro Grande for a critical reading of the manuscript and several useful comments.

[1] N. R. Arista, Stopping of molecules and clusters, Nucl. Instrum. Methods Phys. Res., Sect. B **164-165**, 108 (2000).

[2] H. M. Urbassek, V. Dröge, and R. M. Nieminen, Orientation effects in the stopping of slow dimers in an electron gas, J. Phys.: Condens. Matter **5**, 3289 (1993).

[3] R. Diez Muiño and A. Salin, Energy and angular momentum transfer in the excitation of electron-hole pairs by slow dimers, Phys. Rev. B **62**, 5207 (2000).

[4] N. E. Koval, A. G. Borisov, L. F. S. Rosa, E. M. Stori, J. F. Dias, P. L. Grande, D. Sanchez-Portal, and R. Diez Muiño, Vicinage effect in the energy loss of H_2 dimers: Experiment and calculations based on time-dependent density-functional theory, Phys. Rev. A **95**, 062707 (2017).

[5] R. Garcia-Molina, C. D. Denton, I. Abril, and N. R. Arista, Energy-loss and exit-angle distributions of fragmented H_2^+ ions after traversing carbon foils, Phys. Rev. A **62**, 012901 (2000).

[6] C. Denton, R. Garcia-Molina, I. Abril, G. H. Lantschner, J. C. Eckardt, and N. R. Arista, Effect of the neutral charge fraction in the Coulomb explosion of $H_2{}^+$ ions through aluminum foils, Nucl. Instrum. Methods B **193**, 198 (2002).

[7] S. M. Shubeita, P. L. Grande, J. F. Dias, R. Garcia-Molina, C. D. Denton, and I. Abril, Energy loss of swift H_2 and H_3 molecules in gold: Vicinage effects, Phys. Rev. B **83**, 245423 (2011).

[8] P. Sigmund and A. Schinner, Stopping of swift hydrogen diclusters: Oscillator model, Eur. Phys. J. D **61**, 39 (2011).

[9] A. L. Hoir, C. Cohen, J. J. Ganem, I. Trimaille, I. C. Vickridge, and S. M. Shubeita, Vicinage effect for hydrogen clusters in Si_3N_4 and SiO_2, Phys. Rev. A **85**, 042901 (2012).

[10] G. Wang and Y. Wang, Vicinage effects for a nitrogen molecular cluster in plasmas, Plasma Sci. Technol. **16**, 637 (2014).

[11] W. Brandt, A. Ratkowski, and R. H. Ritchie, Ion Beam Analysis: Fundamentals and Applications, Phys. Rev. Lett. **33**, 1325 (1974).

[12] J. W. Tape, W. M. Gibson, J. Remillieux, R. Laubert, and H. E. Wegner, Energy loss of atomic and molecular ions beams in thin foils, Nucl. Instrum. Methods **132**, 75 (1976).

[13] J. C. Eckardt, G. Lantschner, N. R. Arista, and R. A. Baragiola, Electronic stopping of slow molecular ions in solids, J. Phys. C **11**, L851 (1978).

[14] A. R. Nyaiesh, W. Steckeimacher, and M. W. Lucas, Energy loss of fast H_2 molecules in solids II, J. Phys. C **11**, 2917 (1978).

[15] Y. Horino, Vicinage effects in Rutherford backscattering intensities of MeV clusters ions penetrating thin layers of condensed matter, Nucl. Instrum. Methods Phys. Res., Sect. B **33**, 178 (1988).

[16] Y. Susuki, M. Fritz, K. Kimura, M. Mannami, N. Sakamoto, H. Ogawa, I. Katayama, T. Noro, and H. Ikegami, Stopping power of carbon for 9.6-MeV/amu $H_2{}^+$ ions, Phys. Rev. A **50**, 3533 (1994).

[17] M. Fritz, K. Kimura, Y. Susuki, and M. Mannami, Energy loss of carbon-transmitted 1-MeV $H_2{}^+$ ions, Phys. Rev. A **50**, 2405 (1994).

[18] Y. Susuki, M. Fritz, K. Kimura, M. Mannami, N. Sakamoto, H. Ogawa, I. Katayama, T. Noro, and H. Ikegami, Energy loss and dissociation of 10-MeV/amu $H_3{}^+$ ions in carbon foils, Phys. Rev. A **51**, 3868 (1995).

[19] N. Matsunami, Energy loss distribution of H_2 with 100 keV in thin carbon foils, Nucl. Instrum. Methods Phys. Res., Sect. B **115**, 55 (1996).

[20] B. Touchrift, H. Salah, and N. Benouali, Stopping power of high energy molecular $H_2{}^+$ ions interacting with silicon targets, Nucl. Instrum. Methods Phys. Res., Sect. B **266**, 1177 (2008).

[21] R. C. Fadanelli, P. L. Grande, and G. Schiwietz, Impact-parameter dependence of the energy loss of fast molecular clusters in hydrogen, Phys. Rev. A **77**, 032902 (2008).

[22] A. Lurio, H. H. Andersen, and L. C. Feldman, Search for cluster effects in x-ray production by fast hydrogen molecules, Phys. Rev. A **17**, 90 (1978).

[23] A. Ootuka, F. Fujimoto, K. Komaki, K. Kawatsura, K. Ozawa, and M. Terasawa, Molecular effect of Al K α x-ray yields from aluminum oxide films for H^+ and $H_2{}^+$ ion bombardments, Phys. Lett. A **97**, 191 (1983).

[24] A. Ootuka, K. Kawatsura, K. Komaki, F. Fujimoto, K. Kouchi, and H. Shibata, Molecular effects in KL multiple ionization of Al for H^+ and $H_2{}^+$ ion impacts, Nucl. Instrum. Methods Phys. Res., Sect. B **33**, 304 (1988).

[25] Y. Yamazaki, A. Yasaka, and N. Oda, Molecular and chemical effect in Auger processes induced by molecular ions, Phys. Rev. A **28**, 1873(R) (1983).

[26] S. M. Shubeita, M. A. Sortica, P. L. Grande, J. F. Dias, and N. R. Arista, Signature of plasmon excitations in the stopping ratio of fast hydrogen clusters, Phys. Rev. B **77**, 115327 (2008).

[27] S. M. Shubeita, R. C. Fadanelli, J. F. Dias, P. L. Grande, C. D. Denton, I. Abril, R. Garcia-Molina, and N. R. Arista, Role of electronic excitations in the energy loss of $H_2{}^+$ projectiles in high- materials, Phys. Rev. B **80**, 205316 (2009).

[28] N. R. Arista, Energy loss of correlated charges in an electron gas, Phys. Rev. B **18**, 1 (1978).

[29] G. Basbas and R. H. Ritchie, Vicinage effect in ion-cluster collisions with condensed matter and with single atoms, Phys. Rev. A **25**, 1943 (1982).

[30] T. Kaneko, Inelastic energy loss of H_2^+ and H_3^+ ions correlated with molecular orientation, Phys. Rev. A **51**, 535 (1995).

[31] T. Kaneko, Wave packet theory of bond electrons, Phys. Rev. A **40**, 2188 (1989).

[32] T. Kaneko, Partial and total electronic stoppings of solids and atoms for energetic ions, Phys. Status Solidi B **156**, 49 (1989).

[33] T. Kaneko, Partial and electronic stopping cross sections of atoms and solids for protons, At. Data Nucl. Data Tables **53**, 271 (1993).

[34] J. Lindhard, On the properties of a gas of charged particles, K. Dan. Vidensk. Selsk. Mat. Fys. Medd. **28**, 1 (1954).

[35] Z. H. Levine and S. G. Louie, New model dielectric function and exchange-correlation potential for semiconductors and insulators, Phys. Rev. B **25**, 6310 (1982).

[36] C. C. Montanari, C. D. Archubi, D. M. Mitnik, and J. E. Miraglia, Energy loss of protons in Au, Pb, and Bi using relativistic wave functions, Phys. Rev. A **79**, 032903 (2009).

[37] C. D. Archubi and N. R. Arista, Extended wave packet model to calculate energy loss moments of protons in matter, Phys. Rev. A **96**, 062701 (2017).

[38] N. Bohr, The penetration of atomic particles through matter, K. Dan. Vidensk. Selsk. Mat. Fys. Medd. **18**, 1 (1948).

[39] J. D. Jackson, *Classical Electrodynamics* (John Wiley and Sons, New York, 1975).

[40] P. Sigmund, *Particle Penetration and Radiation Effects* (Springer, New York, 2006).

[41] G. de M. Azevedo, P. L. Grande, and G. Schiwietz, Impact-parameter dependent energy loss of screened ions, Nucl. Instrum. Methods Phys. Res., Sect. B **164-165**, 203 (2000).

[42] A. F. Lifschitz and N. R. Arista, Velocity-dependent screening in metals, Phys. Rev. A **57**, 200 (1998).

[43] W. Brandt and J. Reinheimer, Theory of semiconductor response to charge particles, Phys. Rev. B **2**, 3104 (1970).

[44] H. A. Bethe and R. Jackiw, *Intermediate Quantum Mechanics* (CRC Press, Boca Raton, FL, 1998).

[45] A. D. McLean and R. S. McLean, Roothaan-Hartree-Fock atomic wave functions Slater basis-set expansions for $Z = 2$–54, At. Data Nucl. Data Tables **26**, 197 (1981).

[46] E. Clementi and D. Roetti, Roothaan-Hartree-Fock atomic wavefunctions: Basis functions and their coefficients for ground and certain excited states of neutral and ionized atoms, $Z \leqslant 54$, At. Data Nucl. Data Tables **14**, 177 (1974).

[47] T. Kihara and O. Aono, Unified theory of relaxations in plasmas, I. Basic theorem, J. Phys. Soc. Jpn. **18**, 837 (1963).

[48] C. F. Bunge, J. A. Barrientos, and A. V. Bunge, Roothaan-Hartree-Fock ground-state atomic wave functions: Slater-type orbitals expansions and expectation values for Z=2–54, At. Data Nucl. Data Tables **53**, 113 (1993).

[49] I. Abril, R. Garcia-Molina, N. R. Arista, and C. F. Sanz-Navarro, Electronic energy loss of swift protons in the oxides Al_2O_3, SiO_2 and ZrO_2, Nucl. Instrum. Methods Phys. Res., Sect. B **190**, 89 (2002).

[50] K. Eder, D. Semrad, P. Bauer, R. Golser, P. Maier-Komor, R. Aumay, M. Penalba, A. Arnau, J. M. Ugalde, and P. M. Echenique, Absence of a "Threshold Effect" in the Energy Loss of Slow Protons Traversing Large-Band-Gap Insulators, Phys. Rev. Lett. **79**, 4112 (1997).

[51] M. A. Kumakhov and F. Komarov, *Energy Loss and Ion Ranges in Solids* (Gordon and Breach, New York, 1981).

[52] F. Matias, R. C. Fadanelli, P. L. Grande, N. R. Arista, N. E. Koval, and G. Schiwietz, Stopping power of cluster ions in a free-electron gas from partial-wave analysis, Phys. Rev. A **98**, 062716 (2018).

[53] G. Basbas, W. Brandt, and R. Laubert, Universal cross sections for K-shell ionization by heavy charged particles, I. Low particle velocities, Phys. Rev. A **7**, 983 (1973); W. Brandt and G. Lapicki, L-shell Coulomb ionization by heavy charged particles, *ibid.* **20**, 465 (1979).